Sounding the subsurface of Athabasca Valles using MARSIS radar data: Exploring the volcanic and fluvial hypotheses for the origin of the rafted plate terrain

Joséphine Boisson, Essam Heggy, Stephen Clifford, Alessandro Frigeri, Jeffrey Plaut, William Farrell, Nathaniel Putzig, Giovanni Picardi, Roberto Orosei, Philippe Lognonné, et al.

JOURNAL OF GEOPHYSICAL RESEARCH, VOL. 114, E08003, doi:10.1029/2008JE003299, 2009

Sounding the subsurface of Athabasca Valles using MARSIS radar data: Exploring the volcanic and fluvial hypotheses for the origin of the rafted plate terrain

Joséphine Boisson,[1] Essam Heggy,[1] Stephen M. Clifford,[2] Alessandro Frigeri,[3] Jeffrey J. Plaut,[4] William M. Farrell,[5] Nathaniel E. Putzig,[6] Giovanni Picardi,[7] Roberto Orosei,[8] Philippe Lognonné,[1] and Donald A. Gurnett[9]

Received 12 November 2008; revised 5 May 2009; accepted 26 May 2009; published 21 August 2009.

[1] To test the volcanic and fluvial hypotheses for the origin of the rafted plate terrain observed in the vicinity of Athabasca Valles (5°N, 150°E, Central Elysium Planitia), we investigated the subsurface radar echo from the Mars Advanced Radar for Subsurface and Ionosphere Sounding (MARSIS) 5-MHz band data over this area. The backscattered signal losses were compared to finite difference time domain (FDTD) simulations of those arising from three hypothetical geoelectrical subsurface models, which differed in their assumed composition (percentage basalt versus ice) and assumed mode of origin (fluvial discharge/''frozen sea,'' mudflow, and low-viscosity lavas). The dielectric values used in these models are derived from laboratory measurements of Mars analog materials under Mars-like conditions. FDTD simulations suggest that if the near-surface environment is ice-rich, it will result in an average loss rate of 0.053 dB/m for massive ice (having less than 1% of suspended particulates) and 0.065 dB/m for a mudflow (consisting of a 50/50 mixture of ice and basaltic dust). Whereas the losses associated with a lava flow model increase to 0.19 dB/m. In comparison, the actual signal losses experienced by MARSIS within this region were on the order of 0.18 dB/m within the first 160 m beneath the surface. This suggests that propagation characteristics of Athabasca's near-subsurface are more consistent with a volcanic rather than a fluvial or mudflow origin of the rafted plate terrain, although limitations on radar sounding depth in this region cannot rule out the possibility of more deeply buried massive ice deposits.

Citation: Boisson, J., et al. (2009), Sounding the subsurface of Athabasca Valles using MARSIS radar data: Exploring the volcanic and fluvial hypotheses for the origin of the rafted plate terrain, *J. Geophys. Res.*, *114*, E08003, doi:10.1029/2008JE003299.

1. Introduction

[2] Thermal models of the Martian subsurface suggest that freezing conditions for water may persist from the surface (except at low latitudes where ice is thought to be not stable) to depths ranging from an estimated average of ~3–5 km at the equator to ~8–12 km at the poles, a region known as the cryosphere [*Clifford*, 1993; *Clifford and Parker*, 2001]. At greater depths, any water present will be in a liquid state. Geomorphologic observations of the Martian surface suggest that a substantial amount of water may reside in the subsurface in both ice and liquid form [*Carr*, 1986, 1996]. To assess the potential distribution and state of subsurface water, two low-frequency, nadir-looking, pulse-limited radar sounders, MARSIS (Mars Advanced Radar for Subsurface and Ionosphere Sounding on board the Mars Express spacecraft) and SHARAD (the Shallow Radar instrument on board the Mars Reconnaissance Orbiter) are currently probing the electromagnetic properties of the upper crust.

[3] MARSIS has both an ionospheric and a subsurface sounding mode. In the latter mode, MARSIS operates at four 1-MHz-wide frequency bands centered at 1.8, 3, 4, and 5 MHz [*Picardi et al.*, 2004]. Over this frequency range, MARSIS has a corresponding subsurface vertical resolution of ~50–100 m, depending on the dielectric properties of the medium [*Picardi et al.*, 2004]. For the purpose of this analysis, we have focused on the 5 MHz data as it provides

[1]Equipe Geophysique Spatiale et Planetaire, UMR 7154, Institut de Physique du Globe de Paris, Université de Paris Diderot, CNRS, Paris, France.
[2]Lunar and Planetary Institute, Houston, Texas, USA.
[3]Dipartimento di Scienze della Terra, Università degli Studi di Perugia, Perugia, Italy.
[4]Jet Propulsion Laboratory, California Institute of Technology, Pasadena, California, USA.
[5]NASA Goddard Space Flight Center, Greenbelt, Maryland, USA.
[6]Department of Space Studies, Southwest Research Institute, Boulder, Colorado, USA.
[7]Infocom Department, Università degli Studi di Roma La Sapienza, Rome, Italy.
[8]Istituto di Astrofisica Spaziale e Fisica Cosmica, Istituto Nazionale di Astrofisica, Rome, Italy.
[9]Department of Physics and Astronomy, University of Iowa, Iowa City, Iowa, USA.

0148-0227/09/2008JE003299$09.00

the best vertical resolution (~60 m) and minimizes the effect of ionospheric interference (which increases at lower frequency). MARSIS has a cross-track horizontal resolution of 10–30 km and uses synthetic aperture processing to achieve an along-track resolution of ~5–10 km [*Picardi et al.*, 2004].

[4] Thus, MARSIS has sufficient spatial resolution to investigate the dielectric properties and radar propagation characteristics of the smooth terrain lying to the southwest of Athabasca Valles (5°N, 150°E). This area has been identified as a potential "frozen sea" by *Murray et al.* [2005], as a lava flow field by *Keszthelyi et al.* [2000], *Plescia* [2003], *Werner et al.* [2003], *Keszthelyi et al.* [2004], and *Jaeger et al.* [2007, 2008] or, alternatively, as a frozen mudflow (resulting from the interaction between lava and frozen ground) by *Rice et al.* [2002] and *Page* [2008]. This area has very low surface roughness (average slope across the Central Elysium Planitia is only 0.02% to 0.04% [*Kreslavsky and Head*, 2000]) at the scale of MARSIS wavelengths (from 60 m at 5 MHz to 160 m at 1.8 MHz), greatly reducing the effect of surface clutter and providing optimal conditions for the analysis and interpretation of backscattered surface and subsurface radar signals. Our main aim here is to test the different hypotheses by determining whether the loss rate of the observed backscattered signal in the range direction (i.e., with depth below the surface) is consistent with the presence of frozen sea, frozen mudflow or lava flow. To achieve this goal, we compare the MARSIS backscattered traces with those generated by finite difference time domain (FDTD) radar simulations based on three plausible geoelectrical models of the subsurface, whose dielectric properties have been assigned on the basis of laboratory measurements of Martian analog materials. These models reflect a synthesis of the most recent remote-sensing data and their geologic interpretations by *Berman and Hartmann* [2002], *Burr et al.* [2002], *Rice et al.* [2002], *Plescia* [2003], *Werner et al.* [2003], *Keszthelyi et al.* [2004], *Lanagan* [2004], *Murray et al.* [2005], *Jaeger et al.* [2007], and *Page* [2008] as summarized in section 2. The comparison of observed and simulated data helps quantify how the concentration of ice in the subsurface affects the loss rate of the radar signal (in dB/m), providing an important constraint on the local composition of the subsurface.

2. Geological Context of Southwestern Athabasca Valles

[5] Our study area is located at approximately 5°N and 150°E, in the Central Elysium Planitia (CEP), southwest of Athabasca Valles and Cerberus Fossae, the latter consisting of a long fracture system (Figure 1), that is often identified as the source of water and volcanic materials for this area [*Berman and Hartmann*, 2002; *Rice et al.*, 2002; *Plescia*, 2003]. It is a region that displays some of the youngest widespread evidence of resurfacing activity on Mars [*Berman and Hartmann*, 2002; *Plescia*, 2003], with the most recent events having crater densities consistent with an age of about 30 My [*Werner et al.*, 2003].

[6] High Resolution Stereo Camera (HRSC) images of this area (Figure 2) reveal a surface with a broken, rafted plate morphology [*Murray et al.*, 2005]. Different formation hypotheses have been proposed to explain this appearance.

[7] The first hypothesis is based on a volcanic origin in which a large amount of low-viscosity lava was extruded to form a lava lake [*Keszthelyi et al.*, 2000; *Plescia*, 2003; *Keszthelyi et al.*, 2004; *Jaeger et al.*, 2007]. In the case of lavas, a viscosity below 10^3 Pa s (yield strengths less than 200 Pa) appears necessary to explain the very flat morphology of this area [*Vaucher et al.*, 2009; *Toplis et al.*, 2008]. The cooling and crystallization of the lava should have resulted in the formation of a surface crust that would have fractured and moved in response to the flow of the still liquid lava underneath [*Keszthelyi et al.*, 2004]. The resulting rafted plate morphology would have then been preserved as the lava lake cooled and solidified. The lava flow hypothesis is supported by several other recent data sets. For example, analysis of Thermal Emission Spectrometer (TES) data over different craters in this zone suggests the presence of mafic to ultramafic materials that are most consistent with a basaltic composition [*Stockstill-Cahill et al.*, 2008].

[8] The second hypothesis that we investigate, is the possibility that a large volume of local volcanic material [*Rogers and Christensen*, 2003] has been eroded and mobilized by the catastrophic discharge of groundwater in a low-gradient plain [*Rice et al.*, 2002]. As the mudflow froze, *Rice et al.* [2002] suggest that it would have resulted in the formation of the observed rafted plates. As the ice sublimed, it would have left behind a lag deposit devoid of ice. Although we have investigated this hypothesis, we see no clear mechanism by which such a large volume of volcanic material could have been entrained, and maintained in suspension, to create a low-viscosity mudflow over a very low gradient plain.

[9] The third hypothesis is a fluvial one, which attributes the observed morphology of CEP to the discharge and ponding of a large volume of groundwater. As the surface of the water froze, the resulting ice cover would have been susceptible to fracturing and differential movement in response to any continued flow of the liquid water underneath [*Murray et al.*, 2005]. The subsequent deposition of a thin layer of volcanic ash [*Arvidson et al.*, 2002] or dust [*Keller et al.*, 2006] may have then inhibited the sublimation of the ice sufficiently to allow the survival of ~35 m of the original ~50 m [*Murray et al.*, 2005] of ice to the present-day.

[10] To evaluate the different characteristics of the backscattered echoes expected from these three differing scenarios, we have constructed three corresponding geoelectrical models (illustrated in Figure 3) based on the dielectric properties of analog materials, as measured in the lab. Those models will serve as an input to the FDTD simulation of the radar echoes. The differences and similarities between the radar propagation characteristics of these three models, versus those actually observed by MARSIS, form the basis by which each of the three formation hypotheses will be tested.

3. Local Geoelectrical Context of Athabasca

[11] Understanding the geoelectrical properties of plausible Martian subsurface materials is crucial to interpreting

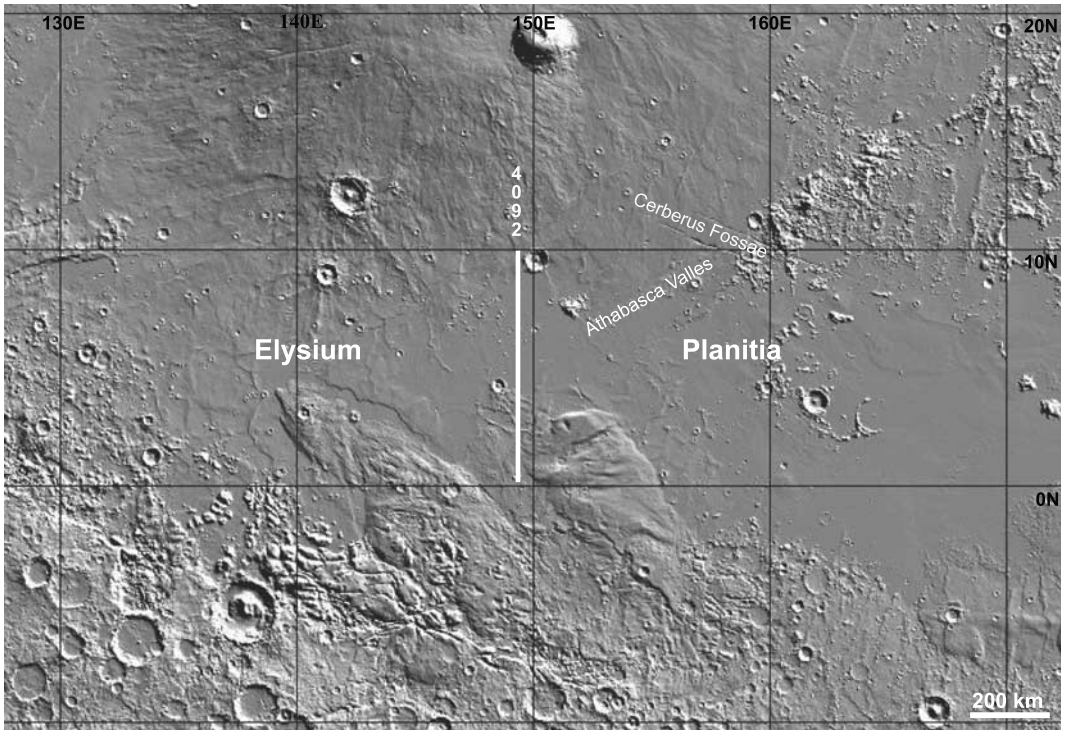

Figure 1. Context map of the Athabasca study area within Central Elysium Planitia (32-pixels/° Mars Orbiter Laser Altimeter shaded relief). The ground track of the MARSIS data acquired on orbit 4092 is indicated by the white line extending from 0.07°N to 9.98°N latitude and from 149.19°E to 149.16°E longitude.

the origin of the reflections and attenuations observed in the MARSIS data. The three geoelectrical models that we constructed are based on the interpretation of data from the Mars Odyssey Gamma Ray Spectrometer (GRS) and Thermal Emission Imaging System (THEMIS), the Mars Global Surveyor TES, and Mars Express HRSC.

[12] *Rogers and Christensen* [2003] suggested that the TES data acquired over the central peak of a large impact crater (~60 km in diameter, ~1150 m deep) located at 9°N, 150°E in the northern part of MARSIS profile 4092 provide evidence that the composition of the exposed bedrock is basaltic (i.e., see Figure 6, region 23 in *Rogers and Christensen*'s [2003] study). This composition is consistent with that inferred for the rest of Elysium Planitia. Thus, for the purpose of our simulations, each of our geoelectrical models (Table 1) is assumed to have a basaltic basement that is 450 m thick in order to prevent reflections from the bottom of the simulation environment.

[13] Recent results from GRS suggest that the Central Elysium Planitia consists of basalt overlain by a thin veneer of dust (a few centimeters to a few tens of centimeters [*Diez et al.*, 2009]). According to the Neutron Spectrometer data, this superficial dust layer is desiccated [*Feldman et al.*, 2004]. While this thin dust or ash layer is considered in our models (Figure 3), its inferred 50 cm thickness is too small to be resolved by the cell size of our simulations and by the ~60 m minimum wavelength of MARSIS. The dielectric contribution of this layer is minimal, so its omission does not influence the simulation results.

[14] Photogeologic estimates suggest that the initial total thickness of the plains-filling material in the CEP region

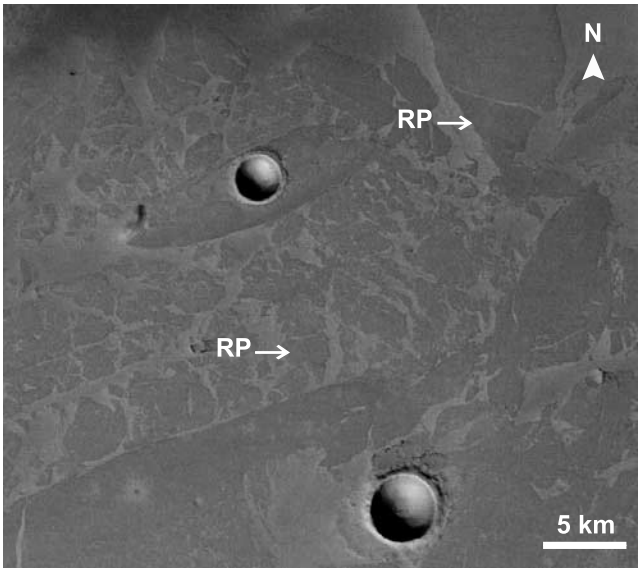

Figure 2. A 25-m resolution HRSC image of the rafted plate (RP) terrain in Athabasca area (centered at 5.5°N, 150°E, Mars Express orbit 32 and image h2165_0001_p13). Arrows indicate samples of rafted plate features with different sizes and locations across the Central Elysium Plain. *Murray et al.* [2005] suggested those formations to be of fluvial origin, while *Jaeger et al.* [2007] and others suggested them to be formed by low-viscosity lava flows.

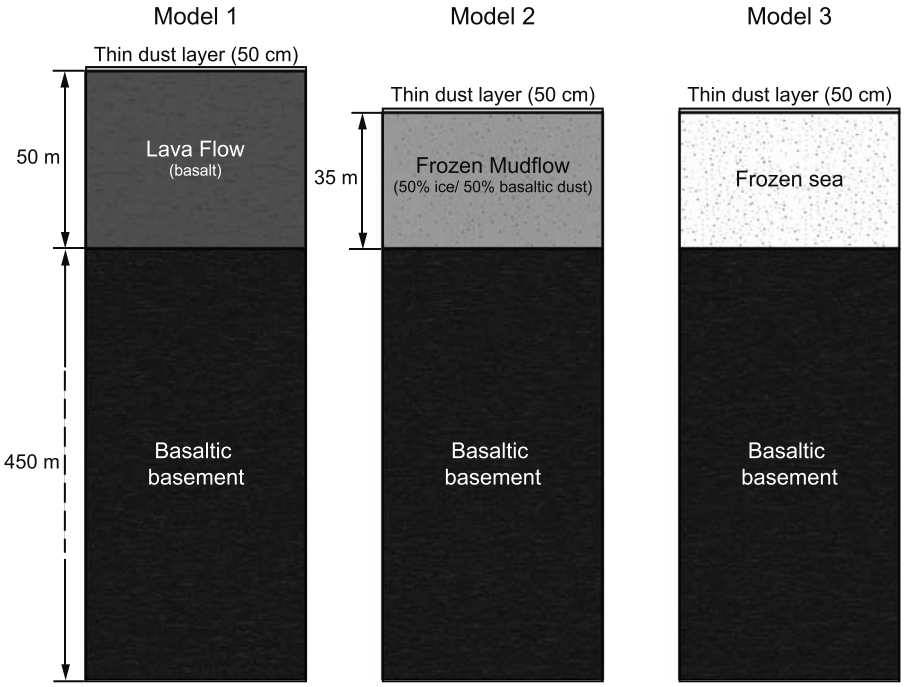

Figure 3. Schematic cross sections of the "lava flow" (Model 1), "frozen mudflow" (Model 2), and "frozen sea" (Model 3) Athabasca geoelectrical models. The dielectric properties of the different geomaterials are presented in Table 1.

was on the order of ~50 m [*Plescia*, 2003; *Keszthelyi et al.*, 2004; *Murray et al.*, 2005]. Therefore, the top layer of our lava flow model (Model 1, Figure 3), is presumed to be basaltic with a thickness of 50 m. For the frozen mudflow model (Model 2, Figure 3), whose composition is assumed to be a 50%/50% mixture of ice and basaltic dust (consistent with the composition of the surrounding plains material), the sublimation of ice is assumed to have depleted 15 m of the original 50 m thickness of the top layer [*Murray et al.*, 2005].

[15] Finally, for the frozen sea model (Model 3, Figure 3), the composition of the upper layer is assumed to be water ice with a 1% content of suspended basaltic particulates. As with the frozen mudflow model, sublimation is assumed to have reduced the original 50 m thickness of the flow to 35 m.

[16] The dielectric properties of each model are summarized in Table 1, where ε' and ε'' are the real and imaginary parts of the dielectric constant and σ is the electrical conductivity of the material. The error associated with the laboratory measurements of ε' and ε'' are 3% and 8%, respectively [*Heggy et al.*, 2007], which, if factored into the propagation calculation, introduce an error in the output signal amplitude of 5%. The theoretical two-way loss rate for most geologic materials (where the real part of the magnetic permeability is equal to 1 and imaginary part is zero) is then given by [*Heggy et al.*, 2006]

$$\alpha = 40\frac{2\pi f}{c}\sqrt{\frac{\varepsilon'}{2}\left[\sqrt{1+\left(\frac{\varepsilon''}{\varepsilon'}\right)^2}-1\right]}, \qquad (1)$$

where c is the free space velocity and f is the wave frequency.

[17] The values presented in Table 1 are taken from laboratory measurements of analog volcanic materials obtained from Craters of the Moon lava field (Idaho, USA), a well-recognized Mars analog environment [*Farr et al.*, 2001; *Heggy et al.*, 2003, 2006, 2007]. For the lava flow layer (in Model 1), the dielectric parameters are 8.05 and 0.37 [*Heggy et al.*, 2006]. For the frozen mudflow layer (in Model 2) and the ice layer (in Model 3), the dielectric parameters are based on *Heggy et al.*'s [2007] work which

Table 1. Dielectric Properties of the Geoelectrical Models[a]

	Layer 1			
Geological Material	Model 1 Lava Flow	Model 2 Frozen Mudflow (50/50 Ice and Basalt)	Model 3 Ice Layer	Layer 2 Basaltic Basement
ε_r'	8.05	3.65	3.10	8.00
ε_r''	0.370	0.117	0.006	0.500
$\sigma \times 10^{-6}$ (S/m)	102.87	32.53	1.72	139.02
Two-way losses (dB/m)	0.273	0.128	0.007	0.370
Thickness (m)	50	35	35	450

[a]Dielectric properties (5 MHz) are based on laboratory measurements of analog materials [*Heggy et al.*, 2003, 2006, 2007]. Here ε_r' and ε_r'' are the real and imaginary part of the relative dielectric constant. The errors on the measurements are 3% for ε_r'' and 8% for ε_r'. Here σ is the conductivity.

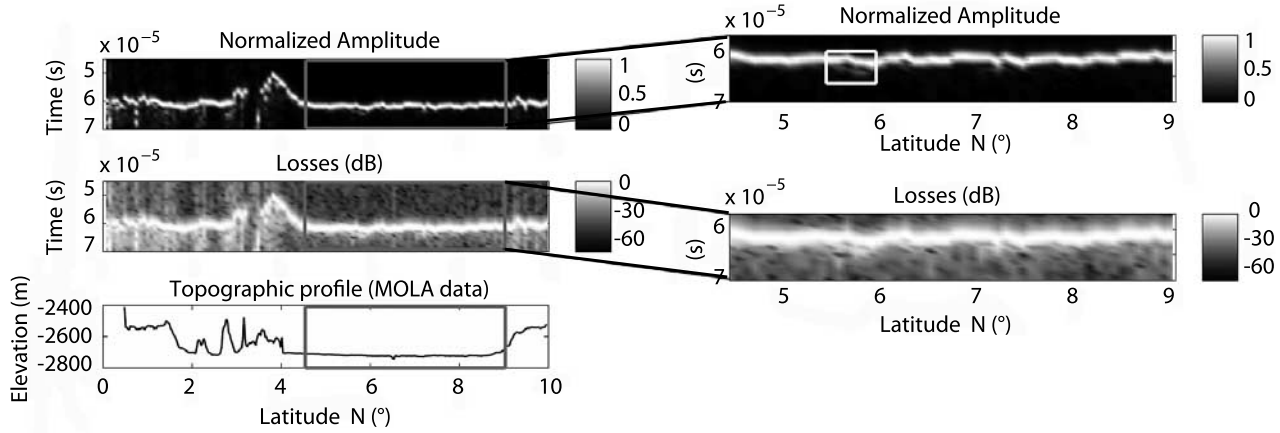

Figure 4. (top) Radargram of the MARSIS 5-MHz data from orbit 4092 (in normalized amplitude). The radar backscattered echoes are plotted in range delay time versus latitude along the ground track. (middle) Radargram for the same observations displayed in losses (dB). (bottom) Corresponding topographic profile along the ground track (128-pixels/° resolution MOLA data). The gray frame corresponds to the flat study area, with enlarged radargrams on the right. The white frame in Figure 4 (top) highlights a reflection that may correspond to a subsurface dielectric discontinuity.

investigates the influence of the ice enrichment in a basaltic matrix on the real and imaginary part of the permittivity. The real and imaginary part of the dielectric constant for the frozen mudflow layer are 3.65 and 0.12, respectively. For the ice layer in our frozen sea model (Model 3), we chose 3.10 and 0.006 as representative values of the real and imaginary parts of the dielectric constant.

4. Ambiguities Associated With Subsurface Reflection Identification

[18] The analysis of low-frequency radar sounding data is often limited by the combined effects of off-nadir and near-nadir clutters due to surface roughness and ionospheric interference. In this analysis, we examine the first 10 μs of the MARSIS backscattered echo in order to determine the signal loss rate (in dB/m) in the near subsurface (first $\sim$160 m). However, because both surface clutter and the ionosphere can influence this near-pulse peak analysis, their relative impact on the signal loss rate must be carefully considered in order to accurately determine the subsurface dielectric contribution. In the discussion that follows, we address the potential effects of surface clutter, the ionosphere, and signal pulse width on our Athabasca loss rate analysis and demonstrate that their influence is minimal.

4.1. Effect of Surface Topography

[19] Surface slopes and near- and off-nadir surface roughness can generate reflections (or clutter) that are visible in the associated radargrams as range-delayed signals that can be mistakenly interpreted as subsurface echoes. The degree to which a rough surface scatters an incident radar wave depends mainly on the signal wavelength. A surface is considered smooth if it satisfies the Rayleigh criterion [*Campbell*, 2002]

$$h_{RMS} < \frac{\lambda}{8\cos\phi}, \tag{2}$$

where λ is the signal wavelength in vacuum (60 m for the 5-MHz band MARSIS signal), ϕ is the incident angle ($\sim$0° for MARSIS), and h_{RMS} is the root mean squared (RMS) height (i.e., square root of the height variance) of the study area. h_{RMS} is given by

$$h_{RMS} = \sqrt{\frac{1}{N^2-1}\sum_{i=1}^{N}\sum_{j=1}^{N}\left(z_{ij}-\tilde{h}\right)^2}, \tag{3}$$

where z_{ij} is the elevation of each point in the two-dimensional $N \times N$ area and $\tilde{h}$ is the mean elevation [*Campbell*, 2002].

[20] To calculate the h_{RMS}, we use the 128 pixels/° Mars Orbiter Laser Altimeter (MOLA) data (horizontal resolution of $\sim$450 m) with a vertical resolution of $\sim$37.5 cm [*Smith and Zuber*, 1998]. At much smaller spatial scale than MOLA, the roughness in this Athabasca area appears to be higher. According to the earth based radiotelescope, the area is rough at decimeter scale [*Harmon et al.*, 1992]. But for the wavelength range of the MARSIS sounder, it is very reasonable to study the topography roughness with MOLA data [*Campbell and Shepard*, 2003]. Thus, we can reasonably assume that this decimeter roughness scale will have an unmeasurable effect on the 5 MHz MARSIS data. For the 5-MHz band MARSIS signal, the Rayleigh criterion is 7.5 m. In comparison, on the basis of the MOLA data, the h_{RMS} for this region (between 4.5°N and 9°N, see enlargement in Figure 4), is 7.1 m. Thus, this area h_{RMS} satisfies the Rayleigh criterion for smoothness, which means that the contribution of off-nadir reflections (clutter) to the observed backscattered echo is very weak.

[21] The second potential topographic effect on the backscattered echo is near-nadir scattering, which depends on both the surface roughness (as defined by the wavelength-scale RMS slope) and the radius of the scattering area [*Campbell and Shepard*, 2003]. The wavelength-scale RMS slope, s_λ, is defined as the RMS height difference

between two points divided by the step-size distance, Δx (which is set equal to the wavelength, on the basis of an interpolation of the MOLA data) [*Orosei et al.*, 2003]

$$s_\lambda = \frac{1}{\Delta x}\sqrt{\frac{1}{n}\sum_{i=1}^{n}[z(x_i) - z(x_i + \Delta x)]^2}, \quad (4)$$

where n is the number of sample points.

[22] The wavelength-scale RMS slope of the studied profile is 0.0015° as calculated from the high-resolution MOLA data. Thus, this area can be considered totally smooth at a scale of ~100 m. Near-nadir scattering depends also on the radius of the scattering area which is 13.4 km for MARSIS [*Campbell and Shepard*, 2003] and on the Hurst exponent, H, which relates the fractal nature of the topography with scale. A low Hurst exponent means that the surface is rough at small scales and becomes increasingly smoother as the scale of interest increases [*Orosei et al.*, 2003]. H varies between 0.2 and 0.35 in the Athabasca area [*Orosei et al.*, 2003]. According to *Campbell and Shepard* [2003], for H = 0.25 and $s_\lambda < 5°$, the coherent component in the near-nadir radar scattering is predominant. Moreover, an illuminated smooth circular area with a radius $\gg\lambda$ (which is the case for Athabasca) presents a backscatter coefficient equal to the polarization-independent Fresnel normal reflectivity (ρ_o) [*Campbell*, 2002]

$$\rho_0 = \left(\frac{\sqrt{\varepsilon_{r2}} - \sqrt{\varepsilon_{r1}}}{\sqrt{\varepsilon_{r2}} + \sqrt{\varepsilon_{r1}}}\right)^2, \quad (5)$$

where ε_{r1} and ε_{r2} are the complex dielectric constants of the upper medium (i.e., the Martian atmosphere, which has a value equal to 1) and the lower medium (assumed to be 7.7 which is the average real permittivity value of the weighted contribution of each layer of the three models). The real part of the backscatter coefficient of the Athabasca area is equal to 0.22. Thus, ~78% of the MARSIS signal is transmitted into the subsurface, demonstrating that the effects of both near-nadir and off-nadir clutter are minimal in the Athabasca area at 5 MHz.

4.2. Ionospheric Distortion

[23] The second type of ambiguity is due to the presence of the ionosphere, which can introduce delays and/or distortion of the MARSIS backscattered signal when the instrument's operating frequency falls near or below the ionosphere's plasma frequency, which varies between 100 kHz to 3.5 MHz, depending on the sun elevation angle [*Safaeinili et al.*, 2003; *Picardi et al.*, 2004]. For the analysis performed here, we chose nighttime (solar angle >90°) data that were acquired at 5 MHz (well above the maximum plasma frequency), thus minimizing the potential for ionospheric interference. As an added precaution, these data were corrected for ionospheric distortion using the "contrast optimization technique" described by *Biccari et al.* [2001], a technique which is known to provide good results for regions that possess low surface roughness at the wavelength scale relevant to MARSIS (~60 to 160 m).

4.3. MARSIS Pulse Width

[24] The third type of effect that can mask the backscattered echo from the subsurface is the MARSIS pulse width. The transmitted pulse width of MARSIS is 250 μs which is much too large to investigate the dielectrical properties of the near subsurface (depths less than several km). However, onboard synthetic aperture processing of the MARSIS data can yield a range compression sufficient to narrow the pulse width to 1 μs under optimal conditions [*Picardi et al.*, 2004]. The amount of compression depends on the local surface roughness, with the narrowest pulse widths resulting from the smoothest surfaces. As discussed in section 4.1, at MARSIS wavelengths (60–160 m), the roughness in the Athabasca area is negligible, resulting in a pulse width that approaches its minimum theoretical value which should be narrow enough to investigate the loss characteristics of the shallow subsurface. This remains true even if the surface roughness at smaller spatial scales is higher. On the basis of this analysis, we can reasonably assume that the MARSIS signal losses observed in Athabasca are attributable to the dielectric properties of the subsurface.

5. Backscattered Loss Comparison

[25] Here we examine the loss rate of the backscattered echoes in the range direction as observed in both the MARSIS data and in our FDTD simulations. For the latter, we converted time into depth on the basis of the real part of the dielectric constant for each of the hypothetical layers (Table 1). For the MARSIS data, we converted the range delay time to depth by using the column-averaged real dielectric constants based on the weighted contributions of the hypothetical layers of each model (~7.7).

[26] For a homogeneous medium, the radar signal attenuation is dominated by dielectric losses, causing it to decline exponentially with depth ($A_z = A_0.e^{-2\alpha z}$ where A is the signal amplitude and α is the attenuation coefficient). Therefore, losses are directly proportional to depth [*Grimm et al.*, 2006]. For a heterogeneous medium, such as a layered subsurface, the signal attenuation is a contribution of both dielectric and scattering losses. When the distance between heterogeneities is greater than the wavelength, the amplitude decrease is characterized by discrete reflections separated by noise [*Grimm et al.*, 2006]. However, if the distance separating the reflectors is lower than the incident signal wavelength, the amplitude (and thus the loss function) shows a continuous decrease with depth [*Heggy et al.*, 2006; *Grimm et al.*, 2006]. The slope of this loss function and the loss rate depend on the resistivity of the medium. Resistive materials, such as those possessing a large volume fraction of ice, have lower loss rates, while conductive ones, such as lava flows, have higher loss rates. In the discussion that follows, we compare the observed and simulated loss functions, using their derived loss rate (in dB/m), to identify the type of attenuations experienced by MARSIS and the true nature of the subsurface.

5.1. MARSIS Data Analysis

[27] For this analysis, we examined three MARSIS profiles (corresponding to orbits 4070, 4081, and 4092), obtained at 4 and 5 MHz, with ground tracks in the vicinity

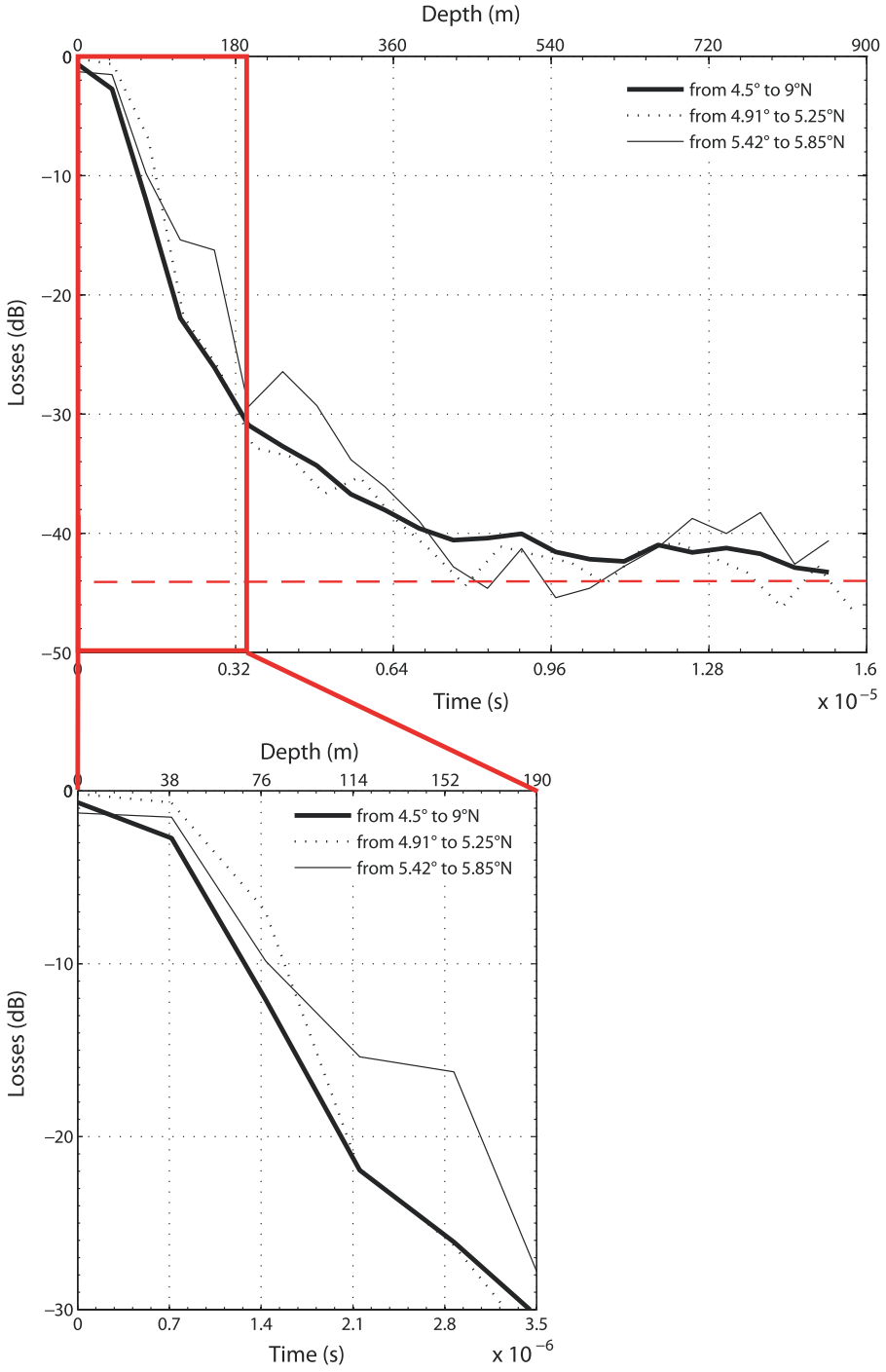

Figure 5. Losses for radar traces between 4.5° and 9°N versus range delay time (s) and depth (m), assuming an average real relative dielectric permittivity of 7.7. The thin black line is the mean of backscattered echoes between 5.42° and 5.85°N, where there is an apparent subsurface signal (see Figure 4). The dotted black line is the mean of backscattered echoes between 4.91° and 5.25°N. The thick black line is the mean of backscattered echoes of the study area between 4.5° and 9°N, omitting the segment from 5.42° to 5.85°N. The dashed red line represents the noise level at −42 dB. The enlargement at the bottom illustrates the loss function in the first 3.5 microseconds (red box).

of Athabasca Valles (5°N, 150°E). Unfortunately, profiles 4070 and 4081 both possess a high noise level, possibly associated with the instrument. Thus, our investigation of Athabasca is based on the analysis of 5 MHz data obtained from Mars Express orbit 4092 which exhibits the best signal-to-noise ratio with no measurable clutter. The profile consists of 119 observations along a track that extends from 0° to 10° N latitude and is centered on 149.17°E longitude (Figure 1). Figure 4 shows the MARSIS radargram for this profile, where the amplitude of the backscattered signal is

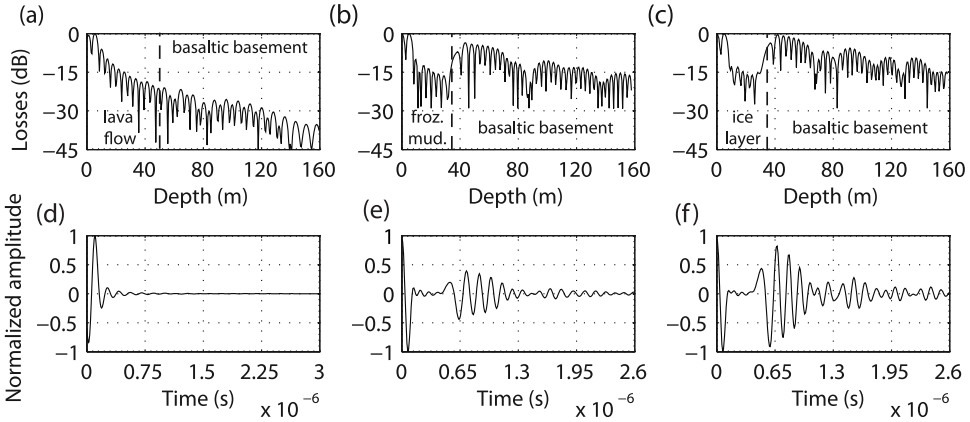

Figure 6. FDTD simulated radar echoes showing (a–c) losses and (d–f) normalized amplitude of the backscattered signal for Model 1 (lava flow model; Figures 6a and 6d), Model 2 (frozen mudflow model, 50% ice/50% basaltic dust; Figures 6b and 6e), and Model 3 (frozen sea model, with a 35-m-thick top layer of ice; Figures 6c and 6f). Black dashed lines represent the interface between the different geoelectrical materials. See Table 1 for material properties. The error on the normalized signal amplitude is 10%.

normalized to the surface return (dimensionless) and the signal losses are expressed in dB. Also shown is the corresponding topographic profile based on the MOLA 128 pixels/° Mission Experiment Gridded Data Records (MEGDR) topography data (version b) [*Smith et al.*, 2001, 2003].

[28] To improve the signal-to-noise ratio, we stacked the radar data between 4.5° and 9°N, summing and averaging over an interval of 5 traces. We also calculated the backscattered signal losses (in dB) as a function of depth, averaged over this same interval (Figure 5), but omitting the segment from 5.42° to 5.85°N, where there is evidence of a subsurface signal (Figure 4, see enlargement). From this analysis, we find the ambient noise level to be ~42 dB (Figure 5, red dashed line), which is in good agreement with the published dynamic range of MARSIS (~30–50 dB [*Picardi et al.*, 2005]). Our main objective here is to study the loss rate (in dB/m) and the nature of the time-range dependency of the decay of backscattered signal amplitude from the shallow subsurface to provide insights regarding the nature and origin of the rafted plate terrain in Athabasca.

5.2. FDTD Backscattered Radar Simulation

[29] To simulate the propagation of the MARSIS signal in the shallow subsurface, we used the FDTD technique [*Yee*, 1966] to solve Maxwell's equations for electromagnetic propagation in discrete steps of time and space, making it possible to study radar wave propagation using parametrical geoelectrical models [*Heggy et al.*, 2003]. The depth of the simulation space is 485 m or 500 m, depending on the model (Table 1 and Figure 3) and its width is 3 km × 3 km, sufficient to reduce multiple scattering from the assumed geometry's sharp edges. In order to maintain the stability of the FDTD simulation, the cell size must be 1/10 of the wavelength or less [*Kunz and Luebbers*, 1993]. According to this criterion, the simulation space was divided into individual cells of 5 × 5 × 5 m. The emitted signal was then modeled as a modulated Gaussian plane wave with a central frequency of 5 MHz. We used this approach to simulate propagation through each of the geoelectrical models.

[30] From the results of our simulations, we obtained the magnitude of the backscattered electric field as a function of propagation time (with an error of 5%), and to maintain consistency with the processing of the MARSIS data, we calculated the signal losses in dB as a function of depth (Figure 6). The plots of the Figure 6 do not look the same as Figure 5. This is explained by the rapid variation in the simulated signal which is due to the modulation in the signal and to the range resolution of the FDTD simulation (which is higher than the MARSIS one and fixed by the simulation stability criterion).

6. Results

[31] Here, we compare the results of our MARSIS data analysis and FDTD simulations to assess the effect of subsurface ice content on the decay of the backscattered radar signal to constrain the likely nature and origin of the Athabasca subsurface.

6.1. MARSIS Data

[32] Between 5.42°N and 5.85°N, the radargram exhibits a secondary subsurface echo at 3 microseconds after the surface reflection (Figure 4, enlargement). Three phenomena could explain the origin of this signal. The first is ionospheric interference, which may produce such an artifact by delaying the signal return. However, as noted earlier, these data were acquired at 5 MHz, well above the nighttime ionospheric plasma frequency, and they were processed to remove the effects of any ionospheric distortion. The second possible explanation for this delayed signal is surface clutter, i.e., an off-nadir reflection originating from the local topography. As discussed in section 4.1, the topographic relief at the MARSIS wavelength in this area is negligible. The third possibility is a reflection from an actual dielectric interface at a depth of ~150–155 m beneath the surface, depending on the dielectric constants of each model.

[33] For this last case, our loss analysis gives different attenuation solutions for the surface and subsurface reflections. For the surface reflection, the loss rate is 0.17 dB/m (calculated for the slope of the thin line between 0.75 to 2.25 microseconds, thin line in Figure 5), while the loss rate associated with the second (subsurface) reflection (Figure 5, slope of the thin line between 3 and 3.5 microseconds) is 0.33 dB/m. These results suggest the presence of two different geologic materials, where the upper "fill" material is less conductive than the basement. Moreover, the losses associated with adjacent terrain (0.27 dB/m, from 4.91° to 5.25°N, dotted line in Figure 5) are similar to those of the subsurface reflection (which is indicative of the composition of the underlying basement between 5.42°N and 5.85°N), implying that they are composed of a similar material. If so, then the most likely explanation for the presence of both surface and subsurface reflection in this region is that it is the result of a depression (centered at 5.6°N) which is filled with a less conductive material.

[34] Calculating the loss rates of the mean backscattered radar echo between 4.5° and 9°N (Figure 5, thick line) yields an average value of 0.18 dB/m for the first 160 m of the subsurface, indicative of a relatively conductive material. Note also that the decline of the loss function is continuous over this depth interval (enlargement, Figure 5), suggesting either a homogeneous subsurface or a heterogeneous subsurface where the distance separating reflectors is lower than the MARSIS wavelength (~20–25 m in the subsurface), possibly consisting of a layered subsurface (see section 5).

6.2. FDTD Simulations

[35] A comparison of the simulated backscattered radar echoes from the three models (one composed of lava flow, the second a basaltic frozen mudflow, 50%/50% ice and basalt, and the third nearly pure ice, simulating a frozen sea) allows us to investigate the influence of subsurface ice content on the propagation of the MARSIS radar signal at 5 MHz. The resulting loss curves (Figures 6a–6c) indicate that, in the first 160 m, the average loss rate for the frozen sea model (Model 3) is smaller than that for the frozen mudflow model (Model 2) and much smaller than that for lava flow model (Model 1).

[36] The average loss rate associated with the lava flow model (Model 1) is 0.19 dB/m (Figures 6a and 6d). In contrast, the average loss rate for the frozen mudflow (Model 2) is 0.065 dB/m (Figures 6b and 6e) and 0.053 dB/m for the frozen sea model (Model 3, Figures 6c and 6f). This low loss is due to the high resistivity of pure ice. The difference in the calculated attenuation between the three geoelectrical models clearly reflects their differing compositions and demonstrates how a higher ice-to-basalt ratio can considerably reduce signal losses.

[37] The losses generated by the frozen sea model increase in a discontinuous way because of the strong dielectric contrasts at the interface between the ice layer and basaltic basement, a contrast that results in multiple reflections within the ice layer. This discontinuous increase is also seen in the frozen mudflow model which also presents a large dielectric contrast. In comparison, the losses associated with the lava flow model increase in a continuous way due to the small dielectric contrast between the lava flow and underlying basaltic basement. Finally, the low losses exhibited by the frozen mudflow model are consistent with the losses expected from a basalt-rich unit possess with a large volume fraction of resistive ice.

7. Discussion

[38] The results of our radar echo simulations suggest that compositional differences in the shallow subsurface can produce measurable differences in signal losses in the MARSIS backscattered echoes, even over depth intervals shorter than the radar signal wavelength. In particular, our simulations suggest that the presence of an ice-rich layer (Models 2 and 3) in the shallow subsurface should significantly reduce the observed loss rate. Even if we reduce the content of ice in the upper layer of the frozen mudflow model (Model 2) down to a minor amount (e.g., 5% in mass), the signal loss rate would remain low compared to the one observed in the lava flow model (Model 1). *Heggy et al.*'s [2007] laboratory measurements suggest that the real and imaginary parts of the dielectric constant for a 5% ice-rich basalt layer are, respectively, 5.2 and 0.26, which are lower than those of the lava flow layer (8.05 and 0.370, respectively).

[39] According to the shape of the MARSIS loss function (see section 6.1), the structure of CEP's shallow (<160 m) subsurface could be either homogeneous or heterogeneous with a distance separating the reflectors lower than the 5 MHz MARSIS wavelength (~20–25 m in the subsurface), thus the limited range sampling in the MARSIS traces prohibits a conclusive assessment. The SHARAD data should help us to constrain the ambiguity on the heterogeneity degree of CEP subsurface.

[40] The observed loss rate of 0.18 dB/m for the MARSIS signal over CEP averaged ~3 times greater than that produced by the two ice-rich subsurface models (frozen sea and frozen mudflow models) in our simulations but very similar to the losses associated with our lava flow model. As discussed above, even reducing to 5% the amount of ice in the frozen mudflow model cannot explain the high signal attenuation rate observed in the MARSIS signal in the CEP area. Moreover, radar signal attenuation study in Deuteronilus Mensae (40°–51°N, 14°–35°E), a region suggested to be composed of an ice-rich subsurface [*Head et al.*, 2006], shows that the average loss rate in this area is 0.013 dB/m [*Plaut et al.*, 2009]. This latest is much lower than that observed in the CEP region (this study). The comparison between those two studies as well as the results of our FDTD simulations demonstrate that the broken, rafted plate terrain in the vicinity of Athabasca is most consistent with a volcanic origin such as fluid lava flows.

[41] Assuming that the subsurface is composed of a volcanic material (with two way loss rate of 0.18 dB/m), we can estimate the maximum sounding depth before the MARSIS signal falls below the ambient noise. Dividing the effective dynamic range of MARSIS (~40 dB) by the mean loss rate of the subsurface (0.18 dB/m), we find that MARSIS can achieve a maximum penetration depth of ~220 m in a volcanic environment.

[42] We are continuing our analysis of additional MARSIS and SHARAD sounding data, supplemented by compositional spectral data from the TES (MGS) and THEMIS

(Mars Odyssey) spectrometers, to further test and constrain the origin of the rafted plate terrain. This study is part of a larger one to test the validity of our loss analysis approach as it applies to the investigation of the potential occurrence and distribution of ground ice and groundwater in the Martian equatorial subsurface.

[43] **Acknowledgments.** We express our gratitude to Vincianne Debaille, Ellen Stoffan, and Bruce Campbell for the helpful discussions and comments. We are grateful to David Baratoux and an anonymous reviewer whose comments and suggestions were of great assistance in the revision of the manuscript. This work was supported in part by NASA grant NRA-02-OSS-01-MARSIS, by the NASA Planetary Geology and Geophysics Program grant NNG05GL11G, and by the Lunar and Planetary Institute CAN-08. Additional French support was provided by CNES and by a MRT Ph.D. grant for J. Boisson. MARSIS is managed by the Agenzia Spaziale Italiana (ASI) and the National Aeronautics and Space Administration (NASA). The Mars Express mission is managed and operated by the European Space Agency (ESA). This is IPGP contribution number 2389 and LPI contribution number 1428.

References

Arvidson, R. E., P. R. Christensen, J. Garvin, and M. Mellon (2002), On the distribution and implications of mantled and exhumed terrains on Mars, paper presented at Solar System Remote Sensing Symposium, Lunar and Planet. Inst., Houston, Tex.

Berman, D. C., and W. K. Hartmann (2002), Recent fluvial, volcanic, and tectonic activity on the Cerberus plains of Mars, *Icarus*, *159*, 1–17, doi:10.1006/icar.2002.6920.

Biccari, D., M. Cartacci, P. Lanza, G. Picardi, D. Quattrocchi, R. Seu, G. Spanò, and P. T. Melacci (2001), Ionosphere phase dispersion compensation, *InfoCom Tech. Rep. 002/005/01*, Univ. of Rome, Rome.

Burr, D. M., J. A. Grier, A. S. McEwen, and L. P. Keszthelyi (2002), Repeated aqueous flooding from the Cerberus plains of Mars, *Icarus*, *159*, 53–73, doi:10.1006/icar.2002.6921.

Campbell, B. A. (2002), *Radar Remote Sensing of Planetary Surfaces*, pp. 29–33, pp. 45–49, pp. 137–138, Cambridge Univ. Press, Cambridge, U. K.

Campbell, B. A., and M. K. Shepard (2003), Coherent and incoherent components in near-nadir radar scattering: Applications to radar sounding of Mars, *J. Geophys. Res.*, *108*(E12), 5132, doi:10.1029/2003JE002164.

Carr, M. H. (1986), Mars: A water-rich planet?, *Icarus*, *68*, 187–216, doi:10.1016/0019-1035(86)90019-9.

Carr, M. H. (1996), *Water on Mars*, Oxford Univ. Press, New York.

Clifford, S. M. (1993), A model for the hydrologic and climatic behavior of water on Mars, *J. Geophys. Res.*, *98*, 10,973–11,016, doi:10.1029/93JE00225.

Clifford, S. M., and T. J. Parker (2001), The evolution of the Martian hydrosphere: Implications for the fate of a primordial ocean and the current state of the northern plains, *Icarus*, *154*, 40–79, doi:10.1006/icar.2001.6671.

Diez, B., W. C. Feldman, N. Mangold, D. Baratoux, S. Maurice, O. Gasnault, L. d'Uston, and F. Costard (2009), Contribution of Mars Odyssey GRS at Central Elysium Planitia, *Icarus*, *200*, 19–29, doi:10.1016/j.icarus.2008.11.011.

Farr, T., et al. (2001), National Research Council planetary decadal study: Terrestrial analogs to Mars, report, Natl. Res. Counc., Washington, D. C.

Feldman, W. C., et al. (2004), Global distribution of near-surface hydrogen on Mars, *J. Geophys. Res.*, *109*, E09006, doi:10.1029/2003JE002160.

Grimm, R. E., E. Heggy, S. Clifford, C. Dinwiddie, R. McGinnis, and D. Farrell (2006), Absorption and scattering in ground-penetrating radar: Analysis of the Bishop Tuff, *J. Geophys. Res.*, *111*, E06S02, doi:10.1029/2005JE002619.

Harmon, J. K., M. P. Sulzer, P. J. Perillat, and J. F. Chandler (1992), Mars Radar mapping strong backscatter from the Elysium Basin and outflow channel, *Icarus*, *95*, 153–156, doi:10.1016/0019-1035(92)90197-F.

Head, J. W., D. R. Marchant, M. C. Agnew, C. I. Fassett, and M. A. Kreslavsky (2006), Extensive valley glacier deposits in the northern mid-latitudes of Mars: Evidence for late Amazonian obliquity-driven climate change, *Earth Planet. Sci. Lett.*, *241*, 663–671, doi:10.1016/j.epsl.2005.11.016.

Heggy, E., P. Paillou, F. Costard, N. Mangold, G. Ruffie, F. Demontoux, G. Grandjean, and J. M. Malézieux (2003), Local geoelectrical models of the Martian subsurface for shallow groundwater detection using sounding radars, *J. Geophys. Res.*, *108*(E4), 8030, doi:10.1029/2002JE001871.

Heggy, E., S. M. Clifford, R. E. Grimm, C. L. Dinwiddie, D. Y. Wyrick, and B. E. Hill (2006), Ground-penetrating radar sounding in mafic lava flows: Assessing attenuation and scattering losses in Mars-analog volcanic terrains, *J. Geophys. Res.*, *111*, E06S04, doi:10.1029/2005JE002589.

Heggy, E., S. M. Clifford, A. Younsi, J. L. Miane, R. Carley, and R. V. Morris (2007), On the dielectric properties of dust and ice-dust mixtures: Experimental characterization of the Martian polar-layered deposits analog materials, *Lunar Planet. Sci.*, *XXXVIII*, abstract 1756.

Jaeger, W. L., L. P. Keszthelyi, A. S. MacEwen, C. M. Dundas, and P. S. Russell (2007), Athabasca Valles, Mars: A lava-draped channel system, *Science*, *317*, 1709–1711, doi:10.1126/science.1143315.

Jaeger, W. L., L. P. Keszthelyi, A. S. MacEwen, C. M. Dundas, and P. S. Russell (2008), Response to "Comment on Athabasca Valles, Mars: A lava-draped channel system," *Science*, *320*, 1588, doi:10.1126/science.1155124.

Keller, J. M., et al. (2006), Equatorial and midlatitude distribution of chlorine measured by Mars Odyssey GRS, *J. Geophys. Res.*, *111*, E03S08, doi:10.1029/2006JE002679, [printed *112*(E3), 2007].

Keszthelyi, L., A. S. McEwen, and T. Thordarson (2000), Terrestrial analogs and thermal models for Martian flood lavas, *J. Geophys. Res.*, *105*(E6), 15,027–15,049, doi:10.1029/1999JE001191.

Keszthelyi, L., T. Thordarson, A. S. McEwen, H. Haack, M.-N. Guilbaud, S. Self, and M. J. Rossi (2004), Icelandic analogs to Martian flood lavas, *Geochem. Geophys. Geosyst.*, *5*, Q11014, doi:10.1029/2004GC000758.

Kreslavsky, M. A., and J. W. Head (2000), Kilometer-scale roughness of Mars: Results from MOLA data analysis, *J. Geophys. Res.*, *105*(E11), 26,695–26,711, doi:10.1029/2000JE001259.

Kunz, K. S., and R. J. Luebbers (1993), *The Finite Difference Time Domain Method for Electromagnetic*, pp. 30–31, CRC Press, Boca Raton, Fla.

Lanagan, P. D. (2004), Geologic history of the Cerberus Plains, Mars, Ph.D. dissertation, Univ. of Ariz., Tucson, Ariz.

Murray, J. B., et al. (2005), Evidence from the Mars Express High Resolution Stereo Camera for a frozen sea close to Mars' equator, *Nature*, *434*, 352–355, doi:10.1038/nature03379.

Orosei, R., R. Bianchi, A. Coradini, S. Espinasse, C. Federico, A. Ferriccioni, and A. I. Gavrishin (2003), Self-affine behavior of Martian topography at kilometer scale from Mars Orbiter Laser Altimeter data, *J. Geophys. Res.*, *108*(E4), 8023, doi:10.1029/2002JE001883.

Page, D. (2008), Comment on "Athabasca Valles, Mars: A lava-draped channel system," *Science*, *320*(5883), 1588, doi:10.1126/science.1154849.

Picardi, G., et al. (2004), Performance and surface scattering models for the Mars Advanced Radar for Subsurface and Ionosphere Sounding (MARSIS), *Planet. Space Sci.*, *52*, 149–156, doi:10.1016/j.pss.2003.08.020.

Picardi, G., et al. (2005), Radar sounding of the subsurface of the Mars, *Science*, *310*, 1925–1928, doi:10.1126/science.1122165.

Plaut, J. J., A. Safaeinili, J. W. Holt, R. J. Phillips, J. W. Head III, R. Seu, N. E. Putzig, and A. Frigeri (2009), Radar evidence for ice in lobate debris aprons in the mid-northern latitudes of Mars, *Geophys. Res. Lett.*, *36*, L02203, doi:10.1029/2008GL036379.

Plescia, J. B. (2003), Cerberus Fossae, Elysium, Mars: A source for lava and water, *Icarus*, *164*, 79–95, doi:10.1016/S0019-1035(03)00139-8.

Rice, J. W., T. J. Parker, A. J. Russel, and O. Knudsen (2002), Morphology of fresh outflow channel deposits on Mars, *Lunar Planet. Sci.*, *XXXIII*, abstract 2026.

Rogers, D., and P. R. Christensen (2003), Age relationship of basaltic and andesitic surface compositions on Mars: Analysis of high-resolution TES observations of the northern hemisphere, *J. Geophys. Res.*, *108*(E4), 5030, doi:10.1029/2002JE001913.

Safaeinili, A., W. Kofman, J. Nouvel, A. Herique, and R. L. Jordan (2003), Impact of Mars ionosphere on orbital radar sounder operation and data processing, *Planet. Space Sci.*, *51*, 505–515, doi:10.1016/S0032-0633(03)00048-5.

Smith, D. E., and M. T. Zuber (1998), The relationship between MOLA northern hemisphere topography and the 6.1-Mbar atmospheric pressure surface of Mars, *Geophys. Res. Lett.*, *25*(24), 4397–4400, doi:10.1029/1998GL900085.

Smith, D. E., et al. (2001), Mars Orbiter Laser Altimeter: Experiment summary after the first year of global mapping of Mars, *J. Geophys. Res.*, *106*(E10), 23,689–23,722, doi:10.1029/2000JE001364.

Smith, D. E., G. A. Neumann, R. E. Arvidson, E. Guinness, and S. Slavney (2003), Mars Global Surveyor Laser Altimeter Mission Experiment Gridded Data Record, http://pds-geosciences.wustl.edu/missions/mgs/megdr.html, Planet. Data Syst., Greenbelt, Md.

Stockstill-Cahill, K. R., F. S. Anderson, and V. E. Hamilton (2008), A study of low-albedo deposits within Amazonis Planitia craters: Evidence for locally derived ultramafic to mafic materials, *J. Geophys. Res.*, *113*, E07008, doi:10.1029/2007JE003036.

Toplis, M. J., M. R. El Maary, D. Baratoux, O. Gasnault, and P. C. Pinet (2008), Are small differences in phosphorous content responsible for

large differences in the composition of Terrestrial and Martian magmatic rocks?, *Lunar Planet. Sci.*, *XXXIX*, abstract 1282.

Vaucher, J., D. Baratoux, M. J. Toplis, P. Pinet, N. Mangold, and K. Kurita (2009), The morphologies of volcanic landforms at Central Elysium Planitia: Evidence for recent and fluid lavas on Mars, *Icarus*, *200*, 39–51, doi:10.1016/j.icarus.2008.11.005.

Werner, S. C., S. Van Gasselt, and G. Neukum (2003), Continual geological activity in Athabasca Valles, Mars, *J. Geophys. Res.*, *108*(E12), 8081, doi:10.1029/2002JE002020.

Yee, K. S. (1966), Numerical solution of initial boundary value problems involving Maxwell equations in isotropic media, *IEEE Trans. Antennas Propag.*, *14*(3), 302–307, doi:10.1109/TAP.1966.1138693.

J. Boisson, E. Heggy, and P. Lognonné, Equipe Geophysique Spatiale et Planetaire, UMR 7154, Institut de Physique du Globe de Paris, Université de Paris Diderot, CNRS, 4 Avenue de Neptune, F-94107 Paris, France. (boisson@ipgp.jussieu.fr; heggy@ipgp.jussieu.fr)

S. M. Clifford, Lunar and Planetary Institute, 3600 Bay Area Boulevard, Houston, TX 77058, USA.

W. M. Farrell, NASA Goddard Space Flight Center, Mail Code 130, Greenbelt, MD 20771, USA.

A. Frigeri, Dipartimento di Scienze della Terra, Università degli Studi di Perugia, I-06123 Perugia, Italy.

D. A. Gurnett, Department of Physics and Astronomy, University of Iowa, Iowa City, IA 52242-1447, USA.

R. Orosei, Istituto di Astrofisica Spaziale e Fisica Cosmica, Istituto Nazionale di Astrofisica, Via del Fosso del Cavaliere 100, I-00133 Rome, Italy.

G. Picardi, Infocom Department, Università degli Studi di Roma La Sapienza, I-00184 Rome, Italy.

J. J. Plaut, Jet Propulsion Laboratory, California Institute of Technology, 4800 Oak Grove Drive, Pasadena, CA 91109, USA. (plaut@mail.jpl.nasa.gov)

N. E. Putzig, Department of Space Studies, Southwest Research Institute, 1050 Walnut Street, Suite 300, Boulder, CO 80302, USA.